Exploring the behaviour of water nanodroplet on a coplanar electrowetting-on-dielectric: a molecular dynamics approach

Hoi Kei Chan[1], *Pui In Mak*[1,2], *Shirley W.I. Siu*[1] ✉

[1]*Department of Computer and Information Science, University of Macau, Avenida da Universidade, Taipa, Macau, People's Republic of China*
[2]*State-Key Laboratory of Analog and Mixed-Signal VLSI, Department of Electrical and Computer Engineering, University of Macau, Avenida da Universidade, Taipa, Macau, People's Republic of China*
✉ *E-mail: shirleysiu@umac.mo*

Published in Micro & Nano Letters; Received on 4th January 2017; Revised on 28th February 2017; Accepted on 1st March 2017

Molecular dynamics simulation has been used to investigate the behaviour of a water nanodroplet on a hydrophobic surface under an applied electric field. The model system mimics a typical electrowetting-on-dielectric experiment of an open-plate coplanar electrodes system. Given the various strengths of the electrode-induced field, variations in contact angle of the droplet, hydrogen bonding and diffusion coefficient of the water molecules are disclosed. Their main findings are: (i) nanodroplet displays asymmetric electrowetting in contact angle measurement; (ii) water molecules and the entire droplet are slightly positively biased; (iii) more water hydrogen bonds are maintained in the positive side, in both the first and the second hydration layer to the surface; and (iv) water diffusion is higher in parallel to the surface than the normal direction.

1. Introduction: Electrowetting-on-dielectric (EWOD) is a popular mechanism to control the spreading of a liquid droplet on a planar dielectric-coated electrode [1, 2]. By altering the electrical signals, a droplet can be actuated to wet or relaxed to dewet the surface in a few milliseconds. This mechanism is employed in digital microfluidics (DMF) to control nano- to microliter droplets on an electrode array independently and precisely by applying a series of electrical potentials. Often, each droplet contains samples and reagents which will be mixed with other droplets in a specific sequence, and transported to the destination cell for measurements and analyses. Due to its high efficiency and versatility, DMF has been applied in lab-on-a-chip systems for a wide variety of applications including proteomics, biochemical assays, and clinical diagnostics [3]. Its wide applicability has motivated research into the fundamental of electrowetting and techniques to improve droplet control [4, 5]. While experimental works have advanced our understanding in many aspects of the electrowetting phenomenon, many questions remain open, and can hardly be solved in the macrodroplet experimental approaches, such as the minimum actuation voltage and contact angle saturation. Since wetting involves molecular rearrangement in the droplet relative to the solid surface, a complete picture cannot be obtained without knowing the structure and dynamics of the molecules comprising the droplet.

In this Letter, we explored the behaviour of a nanoscale water droplet under a range of applied electric fields. Using equilibrium molecular dynamics simulations, we have investigated the variations of contact angle, hydrogen bonding, and water motion of the droplet. Unlike other atomistic MD studies of electrowetting which used uniformed electric field (either perpendicular or parallel field to the surface), we generated an electric field by explicitly simulating a pair of electrodes using a device configuration and surface model similar to those used in EWOD experiment.

2. System and method

2.1. Molecular model: Our simulation system mimics the experimental coplanar open-plate EWOD configuration using a polymer solid surface. As shown in Fig. 1, the solid surface is composed of a hydrophobic monolayer of perfluoro-*n*-decane $C_{10}F_{22}$ molecules (top) and a charging layer of two electrodes (bottom). The choice of the surface molecule is based on the fact that fluoropolymer such as Teflon has been popularly used as coating in EWOD devices for improving hydrophobicity and reducing liquid sticking. The fluorocarbon molecules were arranged in hexagonal shape. In total, 729 flurocarbon molecules were constructed in an area of 196 nm^2 giving a packing density of 0.27 nm^2 per molecule (in accordance with the experimental perfluoroalkane surface density for hexagonal packing on gold [6]). The square electrode at the charging layer was represented as an array of 31×31 atoms with an interatomic spacing of 1 Å. To generate an electric field, a pair of two electrodes was given opposite charges with the same magnitude. Here, the electrode at the positive X direction was designated as the positive electrode while the electrode at the negative X direction was designated as the negative electrode. The gap between two electrodes was 5 Å and the charging layer was vertically separated from the hydrophobic monolayer by ≃8 Å. Placed on top of the hydrophobic surface is a water nanodroplet of 2.6 nm in radius. It is composed of 2228 water molecules previously equilibrated from a cubic box of 4.2 nm^3 and was put near the surface followed by a short period of equilibration. According to the previous study [7], droplet of this size is large enough to yield accurate statistical representation. Without the applied field, the droplet has a contact angle of 125.1°, which is in good agreement with the experimental (advancing) contact angle of 126° [8] of a macrodroplet on the fully fluorinated self-assembled monolayers (SAMs). The size of the simulation box was set as $14 \times 14 \times 30$ nm.

2.2. Simulations: All simulations were performed using the GROMACS 4.5.5 package [9] in canonical ensemble (NVT) ensemble. Periodic boundary conditions were applied in both X and Y directions. In the Z direction, two Lennard–Jones 9-3 potential walls [10] with density of 100 nm^{-3} were added at the top and the bottom of the simulation box to prevent evaporated water to diffuse cross the box boundary.

The system was coupled to a temperature bath at 300 K with a coupling time constant of 0.1 ps^{-1} by velocity rescaling. Bonds to H atoms were constrained using the LINCS algorithm [11] and the integration step size was 2 fs. The non-bonded pair list was updated every 10 steps with a cutoff of 1.2 nm. For the short-range

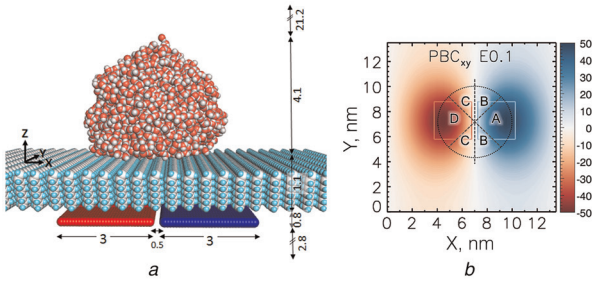

Fig. 1 *Simulation system of nanodroplet on EWOD.*
a Open-plate configuration
b Electric potential induced by two charged electrodes. Droplet location is indicated by dotted line circle and two electrodes by blue (positive) and red (negative) squares; electric potential is displayed as colour heatmap. For contact angle calculation, the droplet was partitioned into four equal-sized regions. Distance measurement is in nm, energy is in kJ/mol

van der Waals interactions, a cutoff distance of 1.0 nm was used. In treating the long-range electrostatics, the Particle-Mesh Ewald [12] with 3DC correction and a grid spacing of 0.12 nm was adopted. The system was simulated with OPLS-AA force field [13] and SPC/E water model.

To investigate the correlation between voltage variations and droplet wetting, the partial charge of the electrode atom was varied systematically. When charged, the electric force generated by two electrodes can be measured using the *g_potential* tool of GROMACS. Here, we name each simulated system with the value of the greatest electric potential measured as presented in Table 1. We emphasise here that the electric field generated by two electrodes is non-uniform. This can be visualised by the changing Coulomb interaction energy between the electrodes and a point charge at various locations of the same plane above the electrodes. Shown in Fig. 1*b* is the heat map of electric potential of a probe atom carrying +1e charge at $Z = 0.5$ nm, which is the first water hydration layer distance to the hydrophobic surface. Electrostatic potential is the strongest around the centre of an electrode and it vanishes in the gap region between the two electrodes. Since electrostatic interaction is long range and the periodic boundary condition was used, we tested the effect from period images by simulating a larger box with size $30 \times 30 \times 30$ nm.

All simulation systems were energy minimised with the steepest descent method and subsequently simulated for 10 ns. Trajectory data was collected every picosecond.

2.3. Analysis: One single measurement which is performed in almost all electrowetting studies is contact angle. Contact angle of the droplet from MD simulations can be calculated using the method described in [14, 15]. Concisely, a two-dimensional water profile outlining the liquid–vapour interface (Gibbs dividing surface) at each horizontal level of the droplet was firstly obtained. Then, the profile was fitted to a circle function to determine the three-phase contact point (liquid–vapour–solid). Finally, the angle between the surface plane and the tangent line to the circle at this point was calculated, which is the contact angle.

Since electrode-induced electric field is non-uniform, droplet wetting will be asymmetric depending on geometry of the electrodes. To give a full picture of the wetting behaviour, we performed contact angle analysis separately on four regions of the droplet (Fig. 1*b*). Regions A and D correspond to parts of the droplet which are most strongly influenced by the positive and the negative electrode, respectively, and less influenced by the oppositely charged electrode; it is because the electric force is inversely proportional to the square of distance. Regions B and C correspond to middle parts of the droplet which are close to both electrodes, hence water molecules in these regions are expected to be strongly influenced by both electrodes.

Existence of a hydrogen bond between two water molecules was decided using a donor–acceptor cutoff distance of 3.5 Å and the acceptor–donor–hydrogen cutoff angle of 30°. Self-diffusion coefficients of water molecules were calculated from the mean square displacement (MSD) of oxygen atoms. Since an applied field from the electrodes below the surface is expected to have different effect on the lateral motion of water molecules from the normal motion, we calculated the lateral (along *XY*-plane) and the normal (along *Z*) diffusion coefficients separately. As MSD curves at long times is known to subject to statistical noise [16], we identified the common initial linear region of the curves (2–10 ps for lateral MSD and 2–30 ps for vertical MSD) and performed fitting accordingly.

Standard errors for all analyses were estimated using block averaging technique [17]: The output data was divided into equal-sized blocks. Then, the mean of each block was calculated and the standard error of the mean was computed as $\sigma/\sqrt{N-1}$ where σ was the standard deviation of the means and N was the total number of blocks. We noticed that all systems were equilibrated within 2 ns, so block averaging was performed on the last 8 ns data using block size of 2 ns.

3. Results and discussion: Fig. 2 shows the final snapshots at $t = 10$ ns of 15 electric field systems and the zero-field system. The initial semi-spherical droplet was observed to spread progressively on the hydrophobic surface as the charge of the electrodes was increased. The droplet is significantly elongated along the *X*-axis (the electrode axis) and simultaneously the height of the droplet is reduced (see also Fig. 4). The change in droplet morphology is related to the geometry of the charged electrodes. Since our device configuration uses a pair of square electrodes, it effectively yields a charged surface of rectangular shape and thus electrowetted droplets will be stretched into elliptical forms. This morphological change is rather drastic in weak field systems. However, for systems with stronger field (E1.7 and above) the shapes of the droplet are not much varied.

Fig. 3 depicts variation of contact angles computed from different parts of the droplet: A and B are spatial regions above the positive electrode (positive side for short), C and D are the negative electrode (negative side). Upon application of an electric field,

Table 1 Simulation systems with applied partial charge on electrode atoms

Sys	*e*	*V*	Sys	*e*	*V*	Sys	*e*	*V*
E0.1	0.0024	0.3	E1.1	0.0270	3.9	E2.1	0.0510	7.4
E0.3	0.0073	1.0	E1.3	0.0310	4.6	E2.3	0.0560	8.1
E0.5	0.0120	1.7	E1.5	0.0370	5.3	E2.5	0.0610	8.8
E0.7	0.0170	2.4	E1.7	0.0410	6.0	E2.7	0.0660	9.5
E0.9	0.0220	3.1	E1.9	0.0460	6.7	E2.9	0.0702	10.2

Charge of $+e$ for atoms in the positive electrode and $-e$ for the atoms in the negative electrode. The system is named by the maximum electric field (in V/nm) generated from the two electrodes. The electrostatic potential yielded across the box (in *V*) is also given for reference

doi: 10.1049/mnl.2016.0824

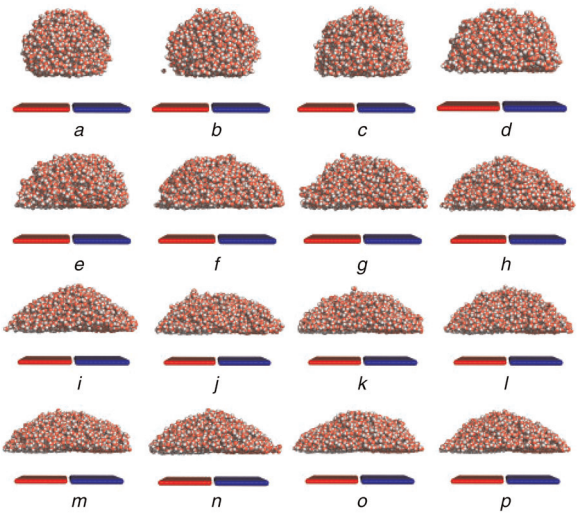

Fig. 2 *Final snapshots of the simulated droplet at different electric field systems. The hydrophobic monolayers have been omitted for clarity*
a, *b*, *c* and *d* E0.0, E0.1, E0.3 and E0.5
e, *f*, *g* and *h* E0.7, E0.9, E1.1and E1.3
i, *j*, *k* and *l* E1.5, E1.7, E1.9, E2.1
m, *n*, *o* and *p* E2.3, E2.5, E2.7, E2.9

contact angles of all regions of the drop decrease almost instantaneously. Again, the changes are more drastic in weak field systems (E0.1 to E1.5) than in strong field systems (E1.7 to E2.9).

Contact angle measured from the positive side can be different from the negative side depending on the field and the material of the surface. This phenomenon has been reported in previous experimental studies [18, 19] and is known as asymmetric electrowetting. Here, asymmetry of contact angle is also observed depending on the field as well as the spatial region. In weaker fields, contact angles of A and D are almost the same; in stronger fields, there is a deviation of 2.8–4.1° where contact angle of A is always smaller than contact angle of D in the same field strength. Similar amount of deviation (1.5–3.5°) can be observed between C and D over a wider range of applied fields. The use of a larger simulation box gives slightly reduced contact angles in moderate-to-weak field systems, but the same asymmetric behaviour is observed.

We remark here that the large contact angle difference between A/D and B/C is presumably due to the geometry of the electrode pair, i.e. longer dimension along *X* and shorter dimension along *Y*. Extending the electrodes at the *Y* dimension will allow the droplet spreading along it and should further lower the contact angles of B and C.

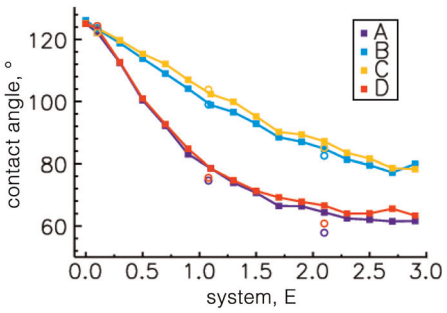

Fig. 3 *Regional contact angle (A, B, C and D, see Fig. 1) in the presence of an applied electric field. Simulation results of larger box size 30 × 30 × 30 are plotted as circle. Standard errors range from 0.11° to 1.0°*

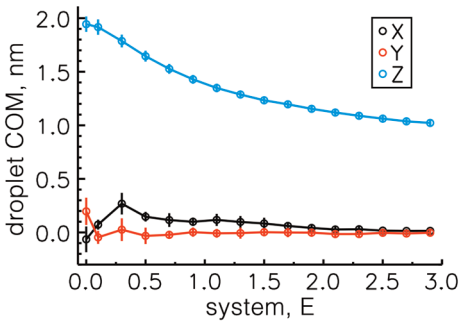

Fig. 4 *Location of the droplet on the surface: X and Y are deviations of the droplet's COM from the middle of the electrode pairs; Z is the distance of COM from the first layer of atoms in the hydrophobic surface. Error bars are standard deviations*

We measured the average centre of mass (COM) of the droplet and counted the number of water molecules to see if there was any location preference of the droplet under applied field. As shown in Fig. 4, the droplet is slightly positively biased: From *X*, the droplet COM is ≃1 Å more to the positive side from the middle of the electrode pair from E0.1 to E1.5. About additional 5–17% (and up to 37% in E0.3, see Fig. 5) of water molecules are located at the positive side in weak field systems (E0.1 to E1.5); in strong field systems, the differences are reduced and the droplet centred at the middle of the electrode pair. We believe that this location preference of water molecules is due to the more favourable water–water interactions in spatial regions close to the positive electrode, as supported by our water hydrogen bond analysis which follows.

Fig. 6 compares the average number of hydrogen bonds per water molecule $\langle n_{HB} \rangle$ at different horizontal layers of the droplet. In the first hydration layer at the solid–liquid interface, $\langle n_{HB} \rangle$ in the positive side increases as a function of applied field, reaching a maximum of 2.88 and saturates at 2.83 in strong fields. Interestingly, in the negative side $\langle n_{HB} \rangle$ is firstly reduced, reaching a minimum of 2.65 and then raised to 2.77, reaching almost the same value as in E0.0. Just one water shell away, in the second hydration layer, $\langle n_{HB} \rangle$ is in the range of the zero-field value of 3.28. Still, water molecules in the positive side are able to maintain more hydrogen bonds than those in the negative side in most electric field systems. Beyond the second hydration layer, the difference is less obvious. Our observations are in line with previous computational studies using uniform external fields. Daub *et al.* [20] observed that a moderate positive perpendicular field enhances hydrogen bonding of solid–liquid interfacial water while negative field suppresses it. Yuan and Zhao [21] also reported a decrease of average water hydrogen bond when stronger negative perpendicular electric field was applied. They showed that in the

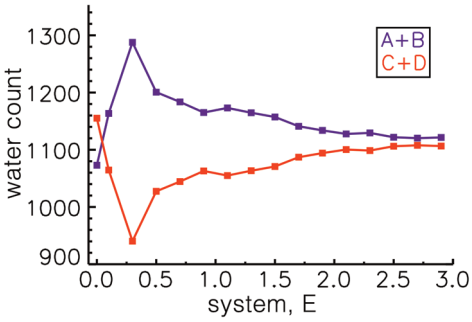

Fig. 5 *Average number of water molecules at the positive electrode side (regions A and B) and at the negative electrode side (regions C and D). Average standard error of E0.1–E1.5 is 27, E1.7–E2.9 is 13*

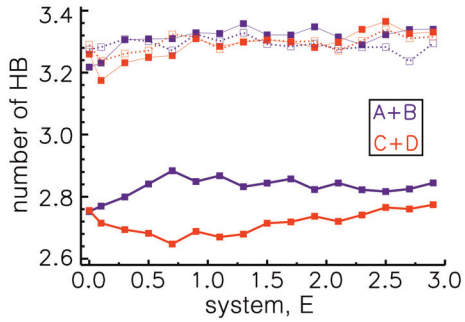

Fig. 6 *Average number of hydrogen bonds per water molecule at different horizontal layers from the hydrophobic surface: the first hydration layer (thick solid line, COM_Z of the water molecule is <5 Å to the hydrophobic surface), the second hydration layer (thin solid line, 5–8 Å), and the third hydration layer of the droplet (dotted line, 8–11 Å). The colour indicates regions of the droplet: the positive side (blue) and the negative side (red)*

first hydration layer, majority of hydrogen bonds are formed within the layer, indicating that a 2D hydrogen bond network was developed [21]. Here, by applying wider range of electric fields, we see that the initial increase and decrease of hydrogen bonds will converge independently to different values at large fields.

Finally, we measured the self-diffusion coefficients (D) of water molecules at the lateral and the normal directions to the hydrophobic surface. We note that D of SPC/E water model in bulk is 2.89 ($\times 10^{-9}$ $m^2 s^{-1}$) [16]; however, in a form of nanodroplet, water molecules were measured to have a D of 3.78, indicating a 30% increase in terms of water mobility. This is very likely because a nanodroplet has a large water–vapour interface. As the number of interfacial hydrogen bonds is reduced, mobility of water molecules is increased due to smaller friction [22]. Putting this nanodroplet in contact with a hydrophobic surface allows even higher mobility of water molecules ($D = 4.33$ in E0.0) (Fig. 7). However, upon application of an electric field, the water motion is suppressed remarkedably. We note here that water mobility along the surface normal is reduced much more (by a factor of 1.1–2.1) than along the lateral direction (1.1–2.7), thus the self-diffusion is anisotropic. Decrease in the dynamics of water under electric field is a consequence of the overall enhancement of the hydrogen bond structure, in particular at the first hydration layer where the water film acts solid like [21].

4. Conclusions: In summary, we have investigated the behaviour of a nanodroplet on an electrode system which is relevant to the experimental configuration in EWOD. Our results demonstrated that like macro-sized water droplet, contact angles of nanodroplet measured at the positive electrode and at the negative electrode are asymmetric depending on the strength of the applied field and

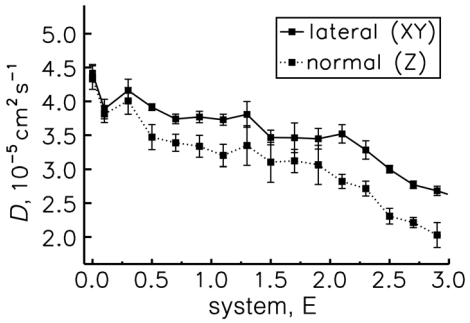

Fig. 7 *Lateral and normal self-diffusion coefficients of water molecules. Error bars are standard errors estimated from block averaging*

region of the droplet measured. Water molecules, and also the droplet as a whole, are positively biased. This can be attributed to the more favourable hydrogen bonding in the positive side than in the negative side. The mobility of water molecules is also affected where the normal motion of water is reduced much more than the lateral motion.

5. Acknowledgment: This project was supported by the State-Key Laboratory of Analog and Mixed-Signal VLSI and granted by University of Macau (grant no. MYRG2014-00104-FST). The authors thank ICTO for their support of computing facilities.

6 References

[1] Mugele F., Baret J.-C.: 'Electrowetting: from basics to applications', *J. Phys.: Condens. Matter*, 2005, **17**, pp. 705–774
[2] Nelson W.C., Kim C.-J.: 'Droplet actuation by electrowetting-on-dielectric (EWOD): a review', *J. Adhes. Sci. Technol.*, 2012, **26**, pp. 1747–1771
[3] Fair R.B.: 'Digital microfluidics: is true lab-on-a-chip possible?', *Microfluid. Nanofluid.*, 2007, **3**, pp. 245–281
[4] Pollack M.G., Shenderov A.D., Fair R.B.: 'Electrowetting-based actuation of droplets for integrated microfluidics', *Lab. Chip*, 2002, **2**, pp. 96–101
[5] Gao J., Liu X., Chen T., *ET AL.*: 'An intelligent digital microfluidic system with fuzzy-enhanced feedback for multi-droplet manipulation', *Lab. Chip*, 2013, **13**, pp. 443–451
[6] Park S.H., Carignano M.A., Nap R.J., *ET AL.*: 'Hydrophobic-induced surface reorganization: molecular dynamics simulations of water nanodroplets on perfluorocarbon self-assembled monolayers', *Soft Mat.*, 2010, **6**, pp. 1644–1654
[7] Song F.H., Li B.Q., Liu C.: 'Molecular dynamics simulation of nano-sized water droplet spreading in an electric field', *Langmuir*, 2013, **29**, pp. 4266–4274
[8] Graupe M., Takenaga M., Koini T., *ET AL.*: 'Oriented surface dipoles strongly influence interfacial wettabilities', *J. Am. Chem. Soc.*, 1999, **121**, pp. 3222–3223
[9] Hess C., Kutzner B., Van Der Spoel D., *ET AL.*: 'GROMACS 4: Algorithms for highly efficient, load-balanced, and scalable molecular simulation', *J. Chem. Theory Comput.*, 2008, **4**, (3), pp. 435–447
[10] Sullivan D.E., Steel G.: 'Structure of simple fluid near the wall', *J. Chem. Phys.*, 1978, **69**, pp. 5420–5459
[11] Hess B., Bekker H., Berendsen H.J.C., *ET AL.*: 'LINCS: a linear constraint solver for molecular simulations', *J. Comput. Chem.*, 1997, **18**, pp. 1463–1472
[12] Yeh I.-C., Berkowitz M.L.: 'Ewald summation for systems with slab geometry', *J. Chem. Phys.*, 1999, **111**, p. 3155
[13] Jorgensen W.L., Maxwell D.S., Tirado-Rives J.: 'Development and testing of the OPLS all-atom force field on conformational energetics and properties of organic liquids', *J. Am. Chem. Soc.*, 1996, **118**, pp. 11225–11236
[14] de Ruijter M.J., Blake T.D., De Coninck J.: 'Dynamic wetting studied by molecular modeling simulations of droplet spreading', *Langmuir*, 1999, **15**, (22), pp. 7836–7847
[15] Werder T., Walther J.H., Jaffe R.L., *ET AL.*: 'On the water-carbon interaction for use in molecular dynamics simulations of graphite and carbon nanotubes', *J. Phys. Chem. B*, 2003, **107**, (6), pp. 1345–1352
[16] Mark P., Nilsson L.: 'Structure and dynamics of the TIP3P, SPC, and SPC/E water models at 298 K', *J. Phys. Chem. A*, 2001, **105**, pp. 9954–9960
[17] Rapaport D.C.: 'The art of molecular dynamics simulation' (Cambridge University Press, 2004)
[18] Fan S.-K., Yang H., Wang T.-T., *ET AL.*: 'Asymmetric electrowetting – moving droplets by a square wave', *Lab. Chip*, 2007, **7**, pp. 1330–1335
[19] Yi U.-C., Kim C.-J.: 'Characterization of electrowetting actuation on addressable single-side coplanar electrodes', *J. Micromech. Microeng.*, 2006, **16**, pp. 2053–2059
[20] Daub C.D., Bratko D., Leung K., *ET AL.*: 'Electrowetting at the nanoscale', *J. Phys. Chem. C*, 2007, **111**, (2), pp. 505–509
[21] Yuan Q., Zhao Y.-P.: 'Precursor film in dynamic wetting, electrowetting, and electro-elasto-capillarity', *Phys. Rev. Lett.*, 2010, **104**, p. 246101
[22] Liu P., Harder E., Berne B.J.: 'On the calculation of diffusion coefficients in confined fluids and interfaces with an application to the liquid-vapor interface of water', *J. Phys. Chem. B*, 2004, **108**, pp. 6595–6602